Biomolecules and Biomedicine
ISSN: 2831-0896 (Print) | ISSN: 2831-090X (Online)
Journal Impact Factor® (2022): 3.4
CiteScore® (2022): 5.3
www.biomolbiomed.com | blog.biomolbiomed.com

RESEARCH ARTICLE **MOLECULAR BIOLOGY**

Impact of *RANGAP1* SUMOylation on Smad4 nuclear export by bioinformatic analysis and cell assays

Feng Zhang[1#], Jun Yang[2#], Yifei Cheng[2*]

[1]Department of Pharmacy, Huashan Hospital, Fudan University, Shanghai, China

[2]Department of Anesthesiology, Huashan Hospital, Fudan University, Shanghai, China

[#]Feng Zhang and Jun Yang contributed equally to this study.

[*]**Corresponding author**: Yifei Cheng; E-mail: yfcheng18@fudan.edu.cn

DOI: https://doi.org/10.17305/bb.2024.10443

Submitted: 06 March 2024/ **Accepted**: 21 May 2024/ **Published online**: 25 May 2024

Conflicts of interest: Authors declare no conflicts of interest.

Funding: Authors received no specific funding for this work.

Data availability: The data that support the findings of this study are available on request from the corresponding author upon reasonable request.

ABSTRACT

Small Ubiquitin-like modifier (SUMOylation) regulates a variety of cellular activities, and its dysregulation has been associated with glioma etiology. The aim of this research was to clarify the function of SUMOylation-related genes in glioma and determine relevant prognostic markers. The Cancer Genome Atlas (TCGA) Glioma and GSE16011 datasets were analyzed through bioinformatics to identify Ran GTPase activating protein 1 (*RANGAP1*) as the hub gene for further study. Experimental validation consisted of quantitative real-time polymerase chain reaction (qRT-PCR), Western blotting (WB), and immunoprecipitation (IP) to evaluate *RANGAP1* expression, function, and interaction with SUMO1. To assess the role of *RANGAP1* knockdown and SUMOylation in glioma cells, various assays were conducted, including cell proliferation, migration, invasion, and apoptosis. In addition, cell cycle analysis and immunofluorescence were performed. Through bioinformatics, *RANGAP1* was identified as a crucial prognostic gene for glioma. Experimental studies confirmed the downregulation of *RANGAP1* in glioma cells and verified that *RANGAP1* repair impedes tumor growth. When it comes to *RANGAP1* silencing, it enhanced cell proliferation, invasion and migration. Additionally, SUMO1 was identified as a specific SUMO molecule coupled to *RANGAP1*, affecting the location of Sma and Mad related protein 4 (Smad4) in the nucleocytoplasm and the transforming growth factor (TGF)-β/Smad signaling pathway. The functional impact of *RANGAP1* SUMOylation on cell proliferation and migration was further confirmed through experiments using a SUMOylation-impairing mutation (K524R). Our findings suggest that *RANGAP1* may be a potential prognostic marker in gliomas and could play a role in regulating cell proliferation, migration, and invasion. SUMOylation of *RANGAP1* is responsible for regulating the TGF-β/Smad signaling pathway, which is crucial for the progression of tumors. Further investigations and experiments are necessary to confirm these results.

KEYWORDS: Glioma, *RANGAP1*, TGF-β/Smad signaling pathway, SUMOylation, SUMO1

INTRODUCTION

Glioma is a common tumor arising in the brain and accounts for a large proportion of primary brain tumors(1). These tumors can be classified based on their cell origin and grade, with glioblastoma multiforme (GBM) being the most aggressive form(2). Environmental and genetic factors contribute to glioma pathogenesis, with exposure to ionizing radiation and certain genetic mutations identified as risk factors(3, 4). The incidence and mortality rates of glioma vary globally, posing a considerable burden on public health(5). Surgery, radiation, and chemotherapy are now available therapeutic methods; nonetheless, the outlook for gliomas remains poor due to their infiltrative nature and low treatment effectiveness(6). Despite extensive research, challenges persist in understanding glioma biology, identifying reliable diagnostic markers, and developing effective treatments. The complex genetic and molecular landscape of gliomas underscores the necessity for continued investigation. Exploring novel diagnostic biomarkers, therapeutic interventions, and prognostic indicators is crucial to advancing glioma research and improving patient outcomes.

Post-translational modification known as SUMOylation, which is the covalent attachment of Small Ubiquitin-like Modifier (SUMO) proteins to particular target proteins, is a crucial process that regulates various cellular functions such as subcellular localization, protein-protein interactions, and protein stability(7, 8). The enzymatic cascade of SUMOylation includes activation by SUMO-activating enzymes (E1), conjugation by SUMO-conjugating enzymes (E2), and ligation by SUMO ligases (E3)(9). The dynamic regulation, mediated by

SUMO-specific proteases, underscores its intricate role in cellular regulatory networks, influencing functions like DNA repair, transcriptional regulation, and genome stability maintenance(10). Dysregulation of SUMOylation has been implicated in various diseases, such as cancer and neurodegenerative disorders. In the context of glioma, Zhu Q et al. revealed a distinctive relationship between SUMOylation and glioma, characterized by heightened Pin1 expression leading to hyperSUMOylation of SUMO1-modified proteins in glioma stem cells(11). Downregulation of SENP1 by Zhang QS et al. hindered glioma cell proliferation and migration while enhancing apoptosis(12). Zhang A et al. emphasized the critical role of elevated SUMO1-modified protein SUMOylation, facilitated by prolyl-isomerase Pin1, in promoting glioblastoma malignancy(13). Furthermore, Yang Y et al. identified the overexpression of SAE1 in glioma tissues, correlating with higher malignancy grades and poor overall survival(14). SAE1 upregulation activated AKT SUMOylation-mediated signaling pathways, promoting glioma progression both in vitro and in vivo. The above examples demonstrate that an in-depth study of SUMOylation in the context of glioma can reveal its impact on disease progression and its potential therapeutic targets. This offers a crucial foundation for more research on the link between SUMOylation and essential genes in glioma.

In this study, we conducted bioinformatics analyses on the GSE16011 dataset and TCGA-glioma dataset using computational biology methods. RANGAP1 was identified as a hub gene through these analyses. Subsequent in vitro experiments explored the interaction between RANGAP1 and the Smad signaling pathway in brain glioma cells. Furthermore, we assessed the impact of RANGAP1 and SUMO1 treatments on the growth of brain glioma cells and the

Smad signaling pathway. These findings shed new light on the therapeutic implications for glioma treatment, providing valuable insights into regulating the effect of RANGAP1 and SUMO1 throughout the course of glioma and their potential as targets for therapeutic interventions.

MATERIALS AND METHODS

Dataset download and processing

The GSE16011 dataset (https://www.ncbi.nlm.nih.gov/gds/?term=GSE16011), which comprising 277 tumor samples and their corresponding 7 controls, was retrieved from the Gene Expression Omnibus (GEO) database (https://www.ncbi.nlm.nih.gov/gds/). Additionally, the Cancer Genome Atlas (TCGA) glioma dataset (https://tcga-data.nci.nih.gov/tcga/), encompassing 666 tumor samples and 5 normal samples, was acquired from the ASSISTANT for Clinical Bioinformatic platform (https://www.aclbi.com/static/index.html). Differential gene expression analysis was conducted on both datasets with the Limma package in the R programming language (The R Foundation for Statistical Computing, Vienna, Austria). Under the criterion of $p< 0.05$, genes with a fold change (FC) greater than 1.5 were considered up-regulated, while genes with an FC less than 0.67 were considered down-regulated(15).

Integration and functional enrichment analysis of intersection genes in glioma datasets

To identify intersectional differentially expressed genes (DEGs) in glioma, the intersection between up- or down-regulated DEGs between the TCGA-glioma dataset and the GSE16011

dataset was analyzed using the Bioinformatics & Evolutionary Genomics website (http://bioinformatics.psb.ugent.be/webtools/Venn/). We downloaded 194 SUMOylation-related genes (Supplementary Table 1) from the article "Novel risk model of three SUMOylation genes based on RNA expression for prediction of potential prognosis and treatment sensitivity of renal cancer". The identified intersection genes were then further intersected with SUMOylation-related genes to obtain a set of key intersection genes. Key intersection genes underwent enrichment analyses with the Kyoto Encyclopedia of Genes and Genomes (KEGG) and Gene Ontology (GO) using the Database for Annotation, Visualization, and Integrated Discovery (DAVID, https://david.ncifcrf.gov/) database; results with $p<0.05$ were deemed statistically significant.

Analysis of prognostic risk model of SUMOylation-related genes in glioma

The "glmnet" program in the R software was used to analyze overlapping genes. The tuning parameters for the Least Absolute Shrinkage and Selection Operator (LASSO) model within the "glmnet" package were determined through ten-fold cross-validation. The optimal λ, representing the minimum criterion for adjusted parameters, was identified to select the most predictive genes. These selected genes, representing the most statistically significant predictors in our dataset, formed the foundation of our prognostic model. Subsequently, the glioma cohort from the TCGA database was stratified into two risk groups based on the expression patterns of the relevant genes. A risk assessment was then conducted for both groups. Kaplan-Meier (KM) analysis was employed to determine the overall survival (OS) probability for the two risk

groups. Additionally, the median survival time was calculated, and survival differences between the two groups were assessed using the log-rank test to derive p values. Hazard ratios (HR) for the high-risk group were also computed to further elucidate relative risk. Ultimately, the "timeROC" software was used to create Receiver Operating Characteristic (ROC) curves, and the Area Under Curve (AUC) values were computed to assess how well the prognostic models predicted patient survival at one, three, and five years. Higher AUC values indicate stronger prognostic prediction capabilities.

Screening of glioma hub genes

Survival analysis was performed based on the KM plotter website (https://www.kmplot.com/) to evaluate the impact of differential expression of 11 selected genes on the OS probability of glioma patients. Log-rank p-values were computed to quantify the statistical significance of observed differences. Subsequently, univariate and multivariate Cox regression analyses, utilizing the forestplot program, were assessed to evaluate the prognostic of the identified genes and specific clinical predictors (age, grade). The calculations included 95% confidence intervals (CIs), hazard ratios (HRs), and p-values for each variable. Variables with p-values less than 0.05 were considered key prognostic factors. Following the identification of key prognostic factors, nomograms were constructed using the rms package to predict 1-year, 3-year, and 5-year survival rates. The concordance index (C-index) was calculated to assess the consistency of the predictions. Calibration curves were generated to visualize the ideal calibration of the nomogram, where closer alignment with the 1-year, 3-year, and 5-year

survival curves indicated better predictive performance. Finally, the expression profiles of the three key genes were investigated using the GSE16011 dataset and TCGA glioma dataset. Wilcoxon tests were employed to assess variations in gene expression between TCGA glioma samples and normal control samples. Raw expression data were processed and visualized using the R programming language, specifically employing the ggplot2 package to generate boxplots illustrating the distribution of gene expression in tumor and normal samples.

Cell lines and culture

The American Type Culture Collection (ATCC) provided the human brain glioma cells U251, SW1783, and U87 to our study. The cells were kept in Dulbecco's Modified Eagle Medium (DMEM), which was enhanced with 10% fetal bovine serum (FBS) and 1% penicillin-streptomycin. HEK293T cells and Human normal brain glial cells (HEB) were also cultured under the same conditions. Cell cultures were maintained in a humidified environment with 5% CO2 at 37°C.

Transfection assay

U251 and U87 cells were seeded in 24-well plates at 2×105 cells per well for transfection. Cells were transfected with three different siRNAs targeting RANGAP1 (si-RANGAP1-1, si-RANGAP1-2, si-RANGAP1-3), with si-NC serving as the negative control. For downregulation of the RANGAP1-SUMO1 complex, a specific siRNA (si-RANGAP1-SUMO1) was used. As directed by the manufacturer, Lipofectamine 3000 was used for the transfections. For experiments assessing the impact of SUMOylation inhibition, the

SUMOylation inhibitors 2-D08 (150 μM for 24 hours) and ML-792 (10 μM for 24 hours) were applied to HEK293T cells.

Plasmid transfection

The eukaryotic expression vector pTango-zeo was used to clone RANGAP1 cDNA, creating the pFlag-RANGAP1 plasmid, which was validated by DNA sequencing. Co-transfection of pHA-UBC9, pFlag-RANGAP1, and His-tagged SUMO plasmids (pHis-SUMO1, pHis-SUMO2, pHis-SUMO3) was performed on HEK293T cells. U251 and U87 cells were treated with varying concentrations of ML-792 (0, 0.2, 0.5, and 1 μM) for 2 hours to evaluate the dose-dependent effects on SUMOylation. Additionally, for three minutes, 100 ng/ml TGF-β was used to activate U251 and U87 cells to investigate the activation of the TGF-β/Smad signaling pathway.

Quantitative real-time polymerase chain reaction (qRT-PCR) assay

According to previous research methods, we conducted qRT-PCR experiments(16). The following primer sequences were used in the amplification process: RANGAP1 forward: 5'-GATCTCACTAGGGGAAGGACTC-3', RANGAP1 reverse: 5'-CACAGTTGTTGAGCTTGAGTTC-3'. SUMO1 forward: 5'-AAAGTCATTGGACAGGATAGCA-3', SUMO1 reverse: 5'-TCTCTGACCCTCAAAGAGAAAC-3'. Similarly, the forward and reverse primers for GAPDH used as the reference gene, were as follows: GAPDH forward: 5′-ATTCCACCCATGGCAAATT-3′, GAPDH reverse: 5′-TGGGATTTCCATTGATGACAAG-3′.

Western blotting (WB) assay

Protease and phosphatase inhibitors were included in RIPA lysis buffer (Thermo Fisher Scientific, USA), which was used to generate cell protein lysates. Cell fractions were prepared by following the manufacturer's instructions for a nuclear/cytoplasmic extraction kit (Thermo Fisher Scientific, USA) in order to separate nuclear and cytoplasmic proteins. The BCA Protein Assay Kit (Thermo Fisher Scientific, USA) was utilized to ascertain the protein content. Proteins in equal quantities were separated using 10% SDS-PAGE and then put onto PVDF membranes from Millipore, USA. Membranes were blocked with 5% skim milk and incubated with primary antibodies (RANGAP1, CDK1, Cyclin B1, Cyclin A2, SUMO1, Smad2/3, Smad4, HSP90, Lamin B1) (Abcam, 1:1000) and appropriate secondary antibodies. Among them, HSP90 and Lamin B1 were used as cytoplasmic and nuclear markers respectively. As an internal reference, GAPDH (Abcam, 1:5000) was employed. Using a ChemiDoc imaging system (Bio-Rad, USA) and an enhanced chemiluminescence (ECL) kit (Thermo Fisher Scientific, USA), protein bands were seen and recorded.

Immunoprecipitation (IP)

Following established protocols, cell lysates containing approximately 2 × 107 cells were ready to extract all of the proteins from immunoprecipitation (IP). To enrich the target protein, 50 μl of anti-Flag M2 affinity gel was incubated overnight at 4 °C with 1-2 mg of protein lysates. To capture the RANGAP1 protein, 2 mg of cellular supernatant was incubated overnight with anti-RANGAP1 antibody-bound protein-A beads. Immunoprecipitation using normal rabbit IgG

was performed as a negative control to account for nonspecific protein binding. The protein complexes were extracted using sample-loading buffer and then put through SDS-PAGE for WB detection after four washes with TBS buffer.

Immunofluorescence (IF) staining

For immunofluorescence examination, U251 and U87 glioma cells were sown on glass coverslips in 24-well plates and left to adhere for 24 hours. After being fixed for 15 minutes at room temperature in 4% paraformaldehyde, the cells were permeabilized for 10 minutes in PBS containing 0.1% Triton X-100. The cells were blocked for an hour with 5% BSA in PBS to prevent non-specific binding, and then they were incubated with primary antibodies against RANGAP1 and SUMO1 for an entire night at 4°C. After incubating with primary antibodies, cells were treated three times with PBS before being incubated for one hour at room temperature in the dark with the corresponding fluorescently tagged secondary antibodies. For five minutes, the nuclei underwent DAPI counterstaining. The coverslips were put onto glass slides using a fluorescent mounting medium following one more round of PBS washings. Confocal laser scanning microscopy was used to capture fluorescence images, and colocalization of RANGAP1 and SUMO1 was analyzed using the merge function of the imaging software by overlaying the respective signals.

Cell counting kit-8 (CCK-8) assay

The proliferation of cells was assessed for vitality using the CCK-8 assay (Dojindo, Japan). In 96-well plates, U251 and U87 cells were planted at a density of 5 × 103 cells per well. After adding CCK-8 reagent to each well, a microplate reader (Thermo Fisher Scientific, USA) was used to measure the absorbance at 450 nm from 0 to 5 days of treatment.

Cell invasion and migration assays

Transwell was used to assess cell invasion and migration. The upper chamber of the Transwell contained transfected brain glioma cells suspended in serum-free medium. Following that, 10% FBS was added to the medium in the lower chamber of the Transwell. After an incubation period, cells with moving cell membranes were stained with DAPI and fixed with 4% paraformaldehyde. Lastly, inverted microscopy was applied to record the number of migratory cells in the field of view. The cell invasion studies were carried out as described previously, with matrigel covered in the upper chamber.

Flow cytometry

For flow cytometric analysis, brain glioma cells were separated using trypsin-EDTA (Gibco, USA) and washed with phosphate-buffered saline (PBS). As directed by the manufacturer, stain cells with Annexin V and propidium iodide (PI) to distinguish between live, apoptotic, and necrotic cells. For the analysis of the cell cycle, cells were fixed, treated with RNase, and stained with PI to evaluate the distribution across cell cycle phases. Analyses were conducted

on a BD Biosciences flow cytometer, and the resulting data were analyzed with FlowJo software (FlowJo LLC, USA) to calculate the percentages of apoptotic cells and to ascertain the cell distribution during the various cell cycle phases.

Statistical analysis

Statistical analysis was conducted using R software. Each experiment was replicated three times in our study, with quantitative data presented as mean ± standard deviation (SD). For normally distributed data, two-tailed Student's t-tests were used to assess group differences; for non-parametric data, Wilcoxon tests were employed. Less than 0.05 was the threshold for statistical significance.

RESULTS

Screening and enrichment analysis of SUMOylation-related genes in glioma

Through the R package, 3498 upregulated and 3172 downregulated DEGs were identified from Glioma samples and normal controls in the TCGA database. 3632 upregulated and 2753 downregulated DEGs from glioma samples and control samples in the GSE16011 dataset (Figures 1A and 1B). Then, 2215 intersectional up-regulated DEGs and 1989 intersectional down-regulated DEGs were identified between the DEGs in TCGA and GSE16011 dataset (Figure 1C). Further intersection analysis identified 50 key intersection genes (Supplementary Table 1) between these DEGs and 194 SUMOylation-related genes (Figure 1D). Subsequent functional enrichment analysis of 50 intersection genes using the DAVID database revealed significant enrichment of Fanconi anemia pathway, cell cycle, and Apoptosis pathways, etc.

(Figure 1E). In GO term, key intersection genes were also related to SUMO Ligase Complex, DNA Binding, NF-kappaB Binding and others (Figure 1F).

Prognostic analysis of 11 signature genes

Utilizing LASSO Cox regression analysis on the 50 intersection genes, we identified 11 signature prognostic genes with significant implications for glioma survival, determined by the optimal lambda value (lambda.min=0.0454) (Figures 2A and 2B). The risk scores for these genes were computed as follows: Riskscore=(-0.4325)*ZEB1+(0.0999)*BRCA1+(0.0795)*HDAC1+(0.025)*BIRC5+(-0.1347)*PCGF2+(0.1656)*CDCA8+(0.3366)*NUP37+(0.1874)*AURKA+(0.0388)*NUP54+(0.1779)*SATB2+(-0.0785)*RANGAP1. In the risk model analysis, the high-risk group showed higher mortality and lower survival (Figure 2C). The results of KM survival analysis showed that the high-risk group had a median survival time of 1.6 years, while the low-risk group had a median survival time of 8 years, and the high-risk group had a lower probability of overall survival (Figure 2D). ROC curve analysis further underscored the predictive accuracy of the risk model, with maximum effectiveness observed at 3 years (AUC=0.922).

Identification of prognostic genes in glioma and selection of RANGAP1 as a potential therapeutic target

In the OS prognosis analysis of the 11 selected signature genes, eight genes exhibited significant prognostic implications (Supplementary Figure 1). Analysis of eight genes and 2

clinical variables in the risk model identified three statistically significant genes ($p<0.05$): BRCA1, HDAC1, and RANGAP1 (Figures 3A and 3B). Nomogram analysis demonstrated that these variables possessed significant predictive power for patients' 1-, 3-, and 5-year survival rates, supported by the calibration curve results (Figures 3C and 3D). How these three genes in TCGA-glioma and GSE16011 datasets are depicted in Figures 3E and 3F. BRCA1 and HDAC1 exhibited significantly elevated expression in tumor samples, while RANGAP1 demonstrated significantly decreased expression in tumor samples. Therefore, due to its prognostic significance and unique expression characteristics, RANGAP1 was selected as the hub gene for subsequent analysis.

Downregulation of RANGAP1 promotes glioma cell growth

qRT-PCR revealed a significant downregulation of RANGAP1 in glioma cells, which was further corroborated by WB analysis indicating lower protein levels (Figures 4A-4C). Subsequently, RANGAP1 knockdown experiments were conducted in U251 and U87 cells, evaluating knockdown efficiency. si-RANGAP1-1 demonstrated superior knockdown efficiency, and it was selected for subsequent experiments (Figures 4D-4F). Functional assays, such as CCK-8 viability and Transwell assays, revealed that the induction of si-RANGAP1-1 significantly enhanced cell proliferation, viability, invasion, and migration abilities (Figures 4G-4L).

RANGAP1 knockdown disrupts cell cycle distribution and inhibits apoptosis in glioma cells

The functional role of RANGAP1 in cell cycle distribution and apoptosis was investigated by downregulating RANGAP1 in glioma cells and analyzing the effects using flow cytometry. The results revealed a significant accumulation of cells in the G2 phase of the cell cycle upon knockdown of RANGAP1 (Figures 5A-5D). Western blot analysis further demonstrated that si-RANGAP1-1 led to a marked increase in the expression levels of cell cycle-related proteins, including CDK1, Cyclin B1, and Cyclin A2, in both U251 and U87 cells (Figures 5E-5G). Additionally, flow cytometry analysis indicated a corresponding decrease in the rate of apoptosis following RANGAP1 knockdown in U251 and U87 cells (Figures 5H and 5I). These findings collectively suggested that RANGAP1 played a crucial role in regulating the cell cycle and programmed cell death in glioma cells.

SUMO1 conjugation modifies RANGAP1

To identify the specific type of SUMO molecule that conjugates with RANGAP1, three exogenous His-tagged SUMO plasmids, and the pFlag-RANGAP1 and pHA-UBC9 plasmids were co-transfected into HEK293T cells. Immunoprecipitation with anti-flag antibody beads revealed that RANGAP1 preferentially forms a complex with UBC9 in the presence of SUMO1. The interaction of SUMO2 and SUMO3 was significantly reduced, indicating a higher specificity of SUMO1 modification (Figure 6A). Similarly, Ni2+-NTA agarose bead purification of His-tagged SUMO conjugates confirmed significant SUMOylation of

RANGAP1 in cells co-transfected with SUMO1, as opposed to SUMO2 or SUMO3 (Figure 6B). Further investigations into the impact of chemical SUMOylation inhibitors on RANGAP1 SUMOylation levels were conducted. Transient transfection of pFlag-RANGAP1 plasmids in HEK293T cells resulted in obvious SUMOylation of exogenously expressed RANGAP1 (Figure 6C). Upon UBC9 stimulation, the abundance of SUMOylated RANGAP1 significantly increased. However, treatment with 150 μM inhibitor 2-D08 for 24 hours led to a significant reduction in SUMOylated RANGAP1, despite the presence of UBC9, attributed to 2-D08 interference with the binding of UBC9 with SUMO1. Additionally, RANGAP1 SUMOylation was also abolished with another SUMOylation inhibitor, ML-792 (10 μM, 24 hours) treatment (Figure 6D). Taken together, these results collectively demonstrate that RANGAP1 was modified through SUMO1 conjugation, which modification is dynamically regulated by SUMO-specific proteases and can be inhibited by 2-D08 or ML-792, emphasizing the specificity and reversibility of RANGAP1 SUMOylation.

Within the TGF-β/Smad signaling cascade, the RANGAP1-SUMO1 complex influences the nucleocytoplasmic distribution of Smad4

Immunofluorescence staining results showed a significant correlation between SUMO and RANGAP1 in U87 and U251 cells. Confocal microscopy images further revealed partial colocalization of SUMO1 and RANGAP1, mainly within the nuclei of glioma cells (Figure 7A). RANGAP1-SUMO1 complex knockdown effectiveness was confirmed by WB analysis and qRT-PCR (Figures 7B and 7C). With knockdown of the RANGAP1-SUMO1 complex, the

protein level of RANGAP1 was also significantly reduced (Figure 7D). The effect of RANGAP1-SUMO1 knockdown on Smad2/3 and Smad4 localization was subsequently analyzed. In U251 cells, we observed that Smad2/3 was mainly retained in the cytoplasmic fraction, whereas Smad4 showed a significant increase in the nuclear fraction after knockdown (Figures 7E and 7F). U87 cells likewise showed similar outcomes (Figures 7G and 7H). These results implied that the RANGAP1-SUMO1 axis played a key role in the regulation of Smad protein distribution in glioma cells, potentially affecting the TGF-β/Smad signaling pathway.

Nuclear export of Smad4 is affected by RANGAP1-SUMO1

To investigate the potential association between SUMOylation and RANGAP1 in the nuclear localization of SUMO1, the selective SUMOylation inhibitor ML-792 was employed. ML-792 specifically targets SUMO activation and has been previously demonstrated to inhibit the formation of RANGAP1-SUMO1 complexes. WB analysis showed a dose-dependent decrease in SUMOylated RANGAP1 levels with increasing concentrations of ML-792 in U251 and U87 cells, but did not affect total RANGAP1 levels (Figures 8A and 8B). SUMO1 level also decreased, this verified the ability of ML-792 to block the SUMO process. To further investigate the effect of SUMO inhibition on Smad signaling, we evaluated the karyoplasmic distribution of Smad2/3 and Smad4 after ML-792 treatment. Following a 2-hour course of therapy with 1 μM ML-792, accumulation of Smad4 was observed in the nuclei of both U87 and U251 cells, resulting in a significant increase in the proportion of Smad4 in the nucleus, while Smad2/3 showed no significant change (Figures 8C-8F). Selective nuclear translocation

of Smad4 after SUMO inhibition suggests that SUMO might be involved in controlling the entry of Smad4 into the nucleus, thereby affecting TGF-β/Smad signaling pathway. These results suggest that inhibition of SUMO by ML-792 disrupts the normal nuclear output of Smad4 and may alter the functional dynamics of the TGF-β/Smad signaling pathway in glioma cells.

RANGAP1 SUMOylation affects Smad4 to inhibit cell proliferation and migration

The structural motifs of the wild-type and mutant RANGAP1 proteins are shown in Figure 9A. Eight leucine-rich repeat regions and high-acidic stretches are present in both proteins. In the mutant RANGAP1, lysine 524 is replaced by arginine, disrupting the SUMOylation site of RANGAP1. The K524R mutation impairs RANGAP1 SUMOylation levels, weakens the interaction between RANGAP1 and SUMO1, and enhances the phosphorylation of SMAD4 in U87 and U251 cells. After stimulation with TGF-β, increased Smad4 phosphorylation was observed in cells expressing wild-type RANGAP1. In contrast, the RANGAP1 K524R mutant exhibited reduced Smad4 phosphorylation, underscoring the importance of SUMOylation in TGF-β mediated Smad signaling (Figure 9B). CCK-8 assays revealed that si-RANGAP1-1 significantly promoted proliferation in U87 and U251 cells, while the K524 mutation weakened this effect (Figures 9C and 9D). Similarly, Transwell assays demonstrated that si-RANGAP1-1 significantly enhanced the migration ability of glioma cells, whereas the K524 mutation attenuated this enhancement (Figures 9E and 9F). These results emphasize the functional implications of the K524R mutation in RANGAP1, impacting cell proliferation and migration

capacities in glioma cells.

DISCUSSION

Gliomas, including glioblastomas, represent a formidable challenge due to their infiltrative nature and limited treatment options(17). Currently, the diagnosis of glioma mainly relies on neuroimaging technology, supplemented by histopathological analysis(18). While these methods provide valuable insights into tumor localization and characteristics, they often lack specificity and sensitivity, leading to challenges in accurate diagnosis and monitoring of disease progression(19). In recent years, targeted gene therapies have emerged as promising strategies for glioma treatment. By exploiting the molecular alterations specific to gliomas, such as mutations in the IDH gene and amplification of the EGFR gene, targeted therapies aim to selectively disrupt pathways crucial for tumor growth and survival(20). Despite initial successes, challenges remain in achieving durable responses and overcoming resistance mechanisms associated with these therapies. Moreover, the five-year survival rate for patients with glioblastoma remains dismal, underscoring the urgent need for innovative approaches to improve prognosis and therapeutic outcomes(21). In this context, the exploration of novel biomarkers holds significant promise for enhancing the precision of glioma diagnosis, guiding personalized treatment strategies, and predicting patient prognosis.

Building on our initial analysis of the GSE16011 dataset and TCGA-glioma dataset, we conducted differential gene screening and enrichment analysis on overlapping genes. The study

by Patil AA and colleagues have previously highlighted a correlation between glioma grade and the Fanconi Anemia pathway, particularly emphasizing FANCD2 re-expression(22). Inhibition of this pathway emerges as a promising strategy to enhance glioma sensitivity to chemotherapeutic agents. Concurrently, the investigation of Yin F et al. underscored the critical role of miR-125a-3p in glioma development, regulating Nrg1 expression directly to affect important processes as apoptosis, proliferation, and migration(23). This positions miR-125a-3p as a potential diagnostic and therapeutic target for malignant glioma. Moreover, the findings of Zou H et al. revealed that 2-Methoxyestradiol (2-ME) enhances radiotherapeutic efficacy in glioma cells by inducing G2/M cell cycle arrest, DNA damage, and activating ATM kinases(24). This substantiates its potential as a radiosensitizer in the treatment of glioblastoma multiform.

Our subsequent analysis focused on the prognosis and expression patterns of overlapping genes and found that three genes with significant prognosis in glioma are BRCA1, HDAC1, and RANGAP1. Among them, some studies have shown that BRCA1 may affect the development of glioma and patient prognosis by regulating the TGF-β/PI3K/AKT/mTOR signaling pathway(25). Another study proposed that BRCA1 expression is regulated by miR-212, affecting radiosensitivity and may affect the efficacy of radiotherapy for glioma(26). HDAC1 overexpression in gliomas is significantly associated with higher tumor grade, poorer prognosis, increased immune infiltration, and is a key component of the prognostic signature. HDAC1 can be a viable treatment target for gliomas as it has been demonstrated to influence cell invasion, proliferation, and apoptosis. Our analysis results showed that BRCA1 and HDAC1

were highly expressed in gliomas, while the expression results of RANGAP1 were opposite. Since there are few studies on RANGAP1 in glioma cell experiments, we selected RANGAP1 as a hub gene for subsequent analysis.

The significance of RANGAP1 in glioma is underscored by its multifaceted roles. Functioning as a GTPase-activating protein for Ran, RANGAP1 orchestrates crucial cellular processes, including nucleocytoplasmic transport, cell cycle progression, and mitotic spindle assembly(27). By accelerating the GTP hydrolysis of Ran, RANGAP1 contributes to proper protein localization and key cellular regulation. In addition to its canonical functions, RANGAP1 is also involved in cell cycle control, microtubule organization, and mitosis, further highlighting its multifunctionality(28). Examining its implications in glioma, RANGAP1 emerges as a pivotal hub gene with potential prognostic significance and dynamic expression patterns. Studies by Zhu S demonstrate the intricate interplay of RANGAP1 with SUMO1, mediated by Ubc9, in translocating from the cytoplasm to nuclear pore complexes(29). Concurrently, Zhao B implicates RANGAP1 in protein SUMOylation, offering a promising avenue for potential inhibitors(30). The regulatory role of RANGAP1, as highlighted by Zhang Z in intracranial aneurysm rupture, adds another layer of complexity, involving the MPO-modulating signaling pathway with miR-877-3p(31). Moreover, the study of Lin TY introduces a potential therapeutic strategy for glioblastoma through oridonin-induced downregulation of RANGAP1 , leading to RNA accumulation and subsequent glioma cell apoptosis(32). Our study found that knocking down RANGAP1 enhanced the proliferation, invasion, and

migration abilities of U251 and U87 cells. Furthermore, the knockdown of RANGAP1 disrupted cell cycle distribution and inhibited apoptosis in glioma cells. Collectively, understanding the multifaceted involvement of RANGAP1 in glioma pathogenesis offers valuable insights for targeted interventions and enhances our comprehension of glioma progression and treatment strategies.

Expanding on the role of SUMO, in post-translational protein modification, it is a crucial participant in various cellular processes, covalently modifying target proteins and influencing their function, stability, or cellular localization(33). The widespread impact of SUMOylation on biological activities, encompassing DNA repair, transcription, and maintenance of genome stability, underscores its significance in shaping cell physiology and disease pathways(34). The research of Wong MB et al. reveals a connection between SUMO-1 and specific lysosomes in neurodegenerative diseases marked by glial protein aggregation, exemplified in multiple system atrophy and progressive supranuclear palsy(35). This association extends to glial cell models expressing α-synuclein, tau, or huntingtin exon 1 mutant, hinting at a potential role for SUMO1 in lysosomal function within the context of glioma-associated protein aggregation. Moreover, the study of Liu X sheds light on the impact of SENP1-mediated de-SUMOylation of SIRT1 in glioma development(36). This process significantly influences cell activity, cycle progression, and apoptosis through the NF-κB pathway, proposing therapeutic implications for gliomas. Zhu et al.'s study revealed the interaction between Peptidyl-prolyl cis/trans isomerase NIMA-interacting 1 (Pin1) and Ubiquitin Specific Peptidase 34 (USP34) in glioma stem cells.

The research indicates that USP34 promoted the isomerization of Ubc9 and protein ubiquitination, while removing the ubiquitination of Pin1, thus stabilizing Pin1. This interaction leads to global high SUMOylation of SUMO1-modified proteins, maintaining the tumorigenic potential of glioma stem cells(37). In alignment with these insights, our investigation contributes to the understanding of SUMO dynamics by uncovering that RANGAP1 undergoes SUMO1 conjugation modification, providing an additional layer of complexity to the intricate landscape of glioma-associated protein modifications.

The Smad signaling pathway, a crucial intracellular cascade transmitting signals from TGF-β ligands, orchestrates diverse cellular processes, encompassing differentiation, growth, and apoptosis(38). In the context of glioma, the investigation of Zhang Q discloses that diminished TGF-β receptor capability, induced by inhibitors, heightens TGF-β ligand synthesis in stem/progenitor cells, fostering proliferation through non-Smad pathways like mTOR and NF-κB(39). At the same time, the research of Yao Z highlights the role of SECTM1 in glioma progression and activates the TGFβ1/Smad signaling pathway, making it a prospective therapeutic target and biomarker(40). In addition, the findings of Zhang C elucidated that the Smad pathway is involved in TGF-β2-induced autophagy, which is critical for glioma invasion by affecting processes such as epithelial-mesenchymal transition and mitochondrial transport, as well as maintaining autocrine loops(41). Based on this, our work demonstrates that RANGAP1 glycosylation inhibits Smad4, hence obstructing cell proliferation and migration, that SUMO1 decrease impacts the nucleocytoplasmic distribution of Smad4, and that the

RANGAP1-SUMO1 complex influences the nuclear export of Smad4. These insights underscored the intricate interplay between SUMOylation, the Smad signaling pathway, and glioma progression, providing a nuanced understanding of potential therapeutic targets in glioma treatment.

CONCLUSION

In summary, this study showed a thorough comprehension of the complex interaction between SUMOylation, the Smad signaling pathway, and glioma progression. The identification of signature prognostic genes, particularly highlighting BRCA1, HDAC1, and RANGAP1, showcased their significant implications for glioma survival. Notably, RANGAP1 emerged as a key regulator affecting crucial cellular processes in glioma cells, shedding light on its potential therapeutic relevance. SUMO1 conjugation is a major modulator of RANGAP1, influencing the nucleocytoplasmic distribution of Smad4 and involving the TGF-β/Smad signaling cascade. The use of SUMOylation inhibitors such as ML-792 shown their potential therapeutic utility in regulating this system. The K524R mutation in RANGAP1 further highlighted its crucial function in cell proliferation and migration, providing insights into glioma biology and opening up new options for targeted therapies.

Authors' contributions

Conception and design of the research: Feng Zhang

Acquisition of data: Jun Yang and Feng Zhang

Analysis and interpretation of data: Feng Zhang

Statistical analysis: Yifei Cheng and Jun Yang

Drafting the manuscript: Jun Yang and Feng Zhang

Revision of manuscript for important intellectual content: Feng Zhang and Yifei Cheng

REFERENCES

1. Lah TT, Novak M, Breznik B, editors. Brain malignancies: Glioblastoma and brain metastases. Seminars in cancer biology; 2020: Elsevier.

2. King JL, Benhabbour SR. Glioblastoma Multiforme—A Look at the Past and a Glance at the Future. Pharmaceutics. 2021;13(7):1053.

3. Masui K, Onizuka H, Cavenee WK, Mischel PS, Shibata N. Metabolic reprogramming in the pathogenesis of glioma: Update. Neuropathology. 2019;39(1):3-13.

4. López GY, Van Ziffle J, Onodera C, Grenert JP, Yeh I, Bastian BC, et al. The genetic landscape of gliomas arising after therapeutic radiation. Acta neuropathologica. 2019;137:139-50.

5. Girardi F, Allemani C, Coleman MP. Worldwide trends in survival from common childhood brain tumors: a systematic review. Journal of global oncology. 2019;5:1-25.

6. Rajaratnam V, Islam MM, Yang M, Slaby R, Ramirez HM, Mirza SP. Glioblastoma: Pathogenesis and current status of chemotherapy and other novel treatments. Cancers. 2020;12(4):937.

7. Salas-Lloret D, González-Prieto R. Insights in post-translational modifications: ubiquitin

and SUMO. International Journal of Molecular Sciences. 2022;23(6):3281.

8. Chen X, Zhang Y, Wang Q, Qin Y, Yang X, Xing Z, et al. The function of SUMOylation and its crucial roles in the development of neurological diseases. The FASEB Journal. 2021;35(4):e21510.

9. Chang H-M, Yeh ET. SUMO: from bench to bedside. Physiological Reviews. 2020;100(4):1599-619.

10. Boulanger M, Chakraborty M, Tempé D, Piechaczyk M, Bossis G. SUMO and transcriptional regulation: the lessons of large-scale proteomic, modifomic and genomic studies. Molecules. 2021;26(4):828.

11. Zhu Q, Liang P, Chu C, Zhang A, Zhou W. Protein sumoylation in normal and cancer stem cells. Frontiers in Molecular Biosciences. 2022;9:1095142.

12. Zhang QS, Zhang M, Huang XJ, Liu XJ, Li WP. Downregulation of SENP1 inhibits cell proliferation, migration and promotes apoptosis in human glioma cells. Oncology Letters. 2016;12(1):217-21.

13. Zhang A, Tao W, Zhai K, Fang X, Huang Z, Yu JS, et al. Protein sumoylation with SUMO1 promoted by Pin1 in glioma stem cells augments glioblastoma malignancy. Neuro-oncology. 2020;22(12):1809-21.

14. Yang Y, Liang Z, Xia Z, Wang X, Ma Y, Sheng Z, et al. SAE1 promotes human glioma progression through activating AKT SUMOylation-mediated signaling pathways. Cell Communication and Signaling. 2019;17:1-14.

15. Rosati D, Palmieri M, Brunelli G, Morrione A, Iannelli F, Frullanti E, et al. Differential

gene expression analysis pipelines and bioinformatic tools for the identification of specific biomarkers: A review. Computational and Structural Biotechnology Journal. 2024;23:1154-68.

16. Zhang X-B, Chen X, Li D-J, Qi G-N, Dai Y-Q, Gu J, et al. Inhibition of miR-155 ameliorates acute kidney injury by apoptosis involving the regulation on TCF4/Wnt/β-catenin pathway. Nephron. 2019;143(2):135-47.

17. Nguyen H-M, Guz-Montgomery K, Lowe DB, Saha D. Pathogenetic features and current management of glioblastoma. Cancers. 2021;13(4):856.

18. Thenuwara G, Curtin J, Tian F. Advances in diagnostic tools and therapeutic approaches for gliomas: A comprehensive review. Sensors. 2023;23(24):9842.

19. Luo J, Pan M, Mo K, Mao Y, Zou D, editors. Emerging role of artificial intelligence in diagnosis, classification and clinical management of glioma. Seminars in Cancer Biology; 2023: Elsevier.

20. Umphlett M, Bilal KH, Martini ML, Suwala AK, Ahuja S, Rashidipour O, et al. IDH-mutant astrocytoma with EGFR amplification—Genomic profiling in four cases and review of literature. Neuro-Oncology Advances. 2022;4(1):vdac067.

21. Korja M, Raj R, Seppä K, Luostarinen T, Malila N, Seppälä M, et al. Glioblastoma survival is improving despite increasing incidence rates: a nationwide study between 2000 and 2013 in Finland. Neuro-oncology. 2019;21(3):370-9.

22. Patil AA, Sayal P, Depondt M-L, Beveridge RD, Roylance A, Kriplani DH, et al. FANCD2 re-expression is associated with glioma grade and chemical inhibition of the Fanconi Anaemia pathway sensitises gliomas to chemotherapeutic agents. Oncotarget. 2014;5(15):6414.

23. Yin F, Zhang JN, Wang SW, Zhou CH, Zhao MM, Fan WH, et al. MiR-125a-3p regulates glioma apoptosis and invasion by regulating Nrg1. PloS one. 2015;10(1):e0116759.

24. Zou H, Zhao S, Zhang J, Lv G, Zhang X, Yu H, et al. Enhanced radiation-induced cytotoxic effect by 2-ME in glioma cells is mediated by induction of cell cycle arrest and DNA damage via activation of ATM pathways. Brain research. 2007;1185:231-8.

25. Wang B, Cao C, Liu X, He X, Zhuang H, Wang D, et al. BRCA1-associated protein inhibits glioma cell proliferation and migration and glioma stem cell self-renewal via the TGF-β/PI3K/AKT/mTOR signalling pathway. Cellular Oncology. 2020;43:223-35.

26. Bahreyni-Toossi M-T, Dolat E, Khanbabaei H, Zafari N, Azimian H. microRNAs: Potential glioblastoma radiosensitizer by targeting radiation-related molecular pathways. Mutation Research/Fundamental and Molecular Mechanisms of Mutagenesis. 2019;816:111679.

27. El-Tanani M, Nsairat H, Mishra V, Mishra Y, Aljabali AA, Serrano-Aroca Á, et al. Ran GTPase and its importance in cellular signaling and malignant phenotype. International Journal of Molecular Sciences. 2023;24(4):3065.

28. Mòdol Cano A. Role of RanGTP and spindle assembly factors in cilia assembly and function. 2021.

29. Zhu S. Analysis of the molecular mechanisms regulating paralogue-specific sumoylation and its effects on protein function: The Johns Hopkins University; 2009.

30. Zhao B, Villhauer EB, Bhuripanyo K, Kiyokawa H, Schindelin H, Yin J. SUMO-mimicking peptides inhibiting protein SUMOylation. ChemBioChem. 2014;15(18):2662-6.

31. Zhang Z, Sui R, Ge L, Xia D. CircRNA_0079586 and circRNA_RanGAP1 are involved in the pathogenesis of intracranial aneurysms rupture by regulating the expression of MPO. Scientific Reports. 2021;11(1):19800.

32. Lin T-Y, Lee C-C, Chen K-C, Lin C-J, Shih C-M. Inhibition of RNA transportation induces glioma cell apoptosis via downregulation of RanGAP1 expression. Chemico-biological interactions. 2015;232:49-57.

33. Han Z-J, Feng Y-H, Gu B-H, Li Y-M, Chen H. The post-translational modification, SUMOylation, and cancer. International journal of oncology. 2018;52(4):1081-94.

34. Zilio N, Eifler-Olivi K, Ulrich HD. Functions of SUMO in the Maintenance of Genome Stability. SUMO Regulation of Cellular Processes. 2017:51-87.

35. Wong MB, Goodwin J, Norazit A, Meedeniya AC, Richter-Landsberg C, Gai WP, et al. SUMO-1 is associated with a subset of lysosomes in glial protein aggregate diseases. Neurotoxicity research. 2013;23:1-21.

36. Liu X, Zhang S, Dong Y, Xie Y, Li Q. SENP1-mediated SUMOylation of SIRT1 affects glioma development through the NF-κB pathway. Experimental Cell Research. 2023;433(2):113822.

37. Zhu Q, Liang P, Meng H, Li F, Miao W, Chu C, et al. Stabilization of Pin1 by USP34 promotes Ubc9 isomerization and protein sumoylation in glioma stem cells. Nature Communications. 2024;15(1):40.

38. Tzavlaki K, Moustakas A. TGF-β Signaling. Biomolecules. 2020;10(3):487.

39. Zhang Q, Guo W, Di C, Lou M, Li H, Zhao Y. Effects of transforming growth factor-β

inhibitor on the proliferation of glioma stem/progenitor cell. Polish Journal of Pathology. 2017;68(4):312-7.

40. Yao Z, Zhang F, Qi C, Wang C, Mao M, Zhao C, et al. SECTM1 promotes the development of glioblastoma and mesenchymal transition by regulating the TGFβ1/Smad signaling pathway. International Journal of Biological Sciences. 2024;20(1):78.

41. Zhang C, Zhang X, Xu R, Huang B, Chen A-J, Li C, et al. RETRACTED ARTICLE: TGF-β2 initiates autophagy via Smad and non-Smad pathway to promote glioma cells' invasion. Journal of Experimental & Clinical Cancer Research. 2017;36(1):1-15.

TABLES AND FIGURES WITH LEGENDS

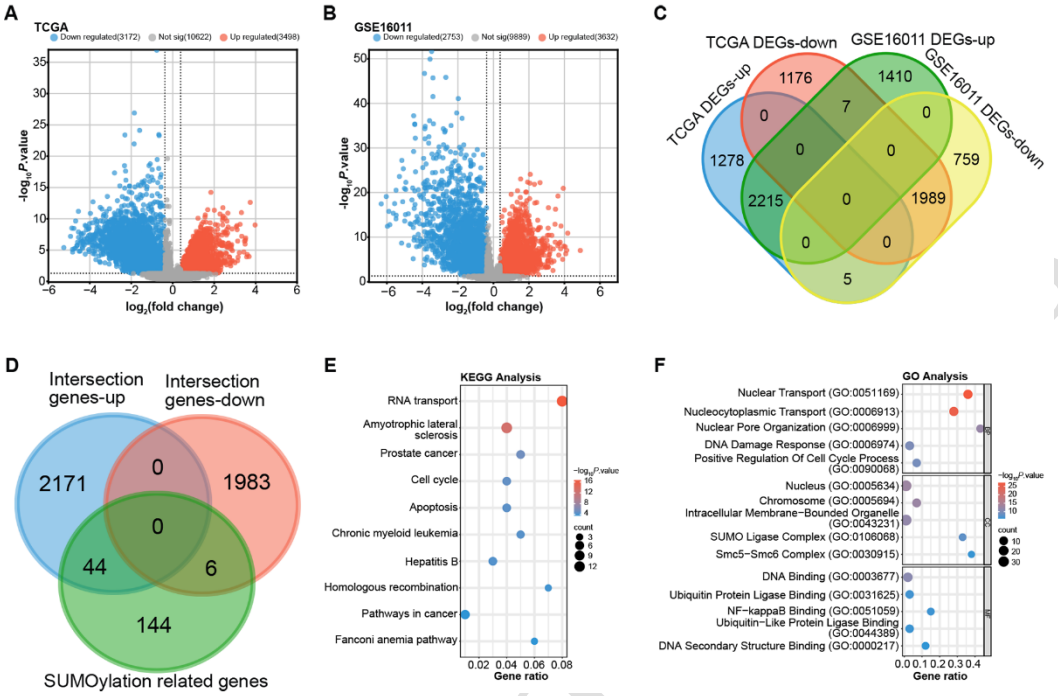

Figure 1. **Identification and enrichment analysis of SUMOylated genes in glioma.** (A and B) Volcano plots of DEGs for TCGA-glioma and GSE16011 datasets. Orange represents up-regulated genes, blue represents down-regulated genes, and gray represents insignificant genes. (C) Venn diagram obtained by the intersection of the up-regulated DEGs of TCGA and the up-regulated DEGs of the GSE16011 dataset, as well as the intersection of the down-regulated DEGs of TCGA and the down-regulated DEGs of the GSE16011 dataset. (D) Venn diagram obtained by the intersection of intersection genes-up, intersection genes-down, and SUMOylation-related genes. (E and F) Top 10 enriched KEGG pathways (E) and 15 GO terms (F). The x-axis represents the Gene Ratio; the y-axis represents the GO Term or enriched pathway; the size of the dots represents the odds ratio; the color of the dots represents the level of the p-value.

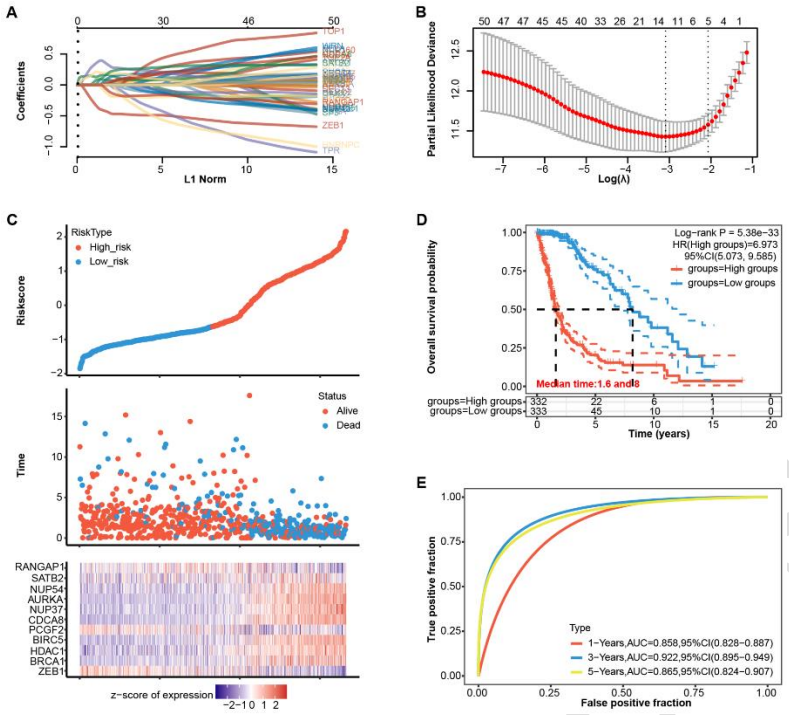

Figure 2. **Prognostic risk model analysis of SUMOylation-related genes in glioma.** (A) LASSO-Cox regression model analysis of SUMOylation-related genes in glioma, different colored lines represent different genes. (B) The relationship between 10-fold cross-validation partial likelihood deviation and log(λ). The leftmost vertical line represents the optimal lambda value that minimizes the cross-validation error, and the right vertical line represents the lambda value "within 1 standard error." (C) Conduct risk model analysis on selected sample data. The upper image shows the risk score distribution of the high-risk group and the low-risk group, the middle image shows the survival status of different risk groups, and the lower image is a heat map of the cluster distribution of characteristic genes. (D) The KM survival curve analysis of the two groups in the risk model, the red line indicates the high-risk group and the green line indicates the low-risk group. (E) ROC curve analysis on the risk model in patients at 1, 3, and 5 years, the horizontal coordinate is a false positive fraction, and the vertical coordinate is a true positive fraction.

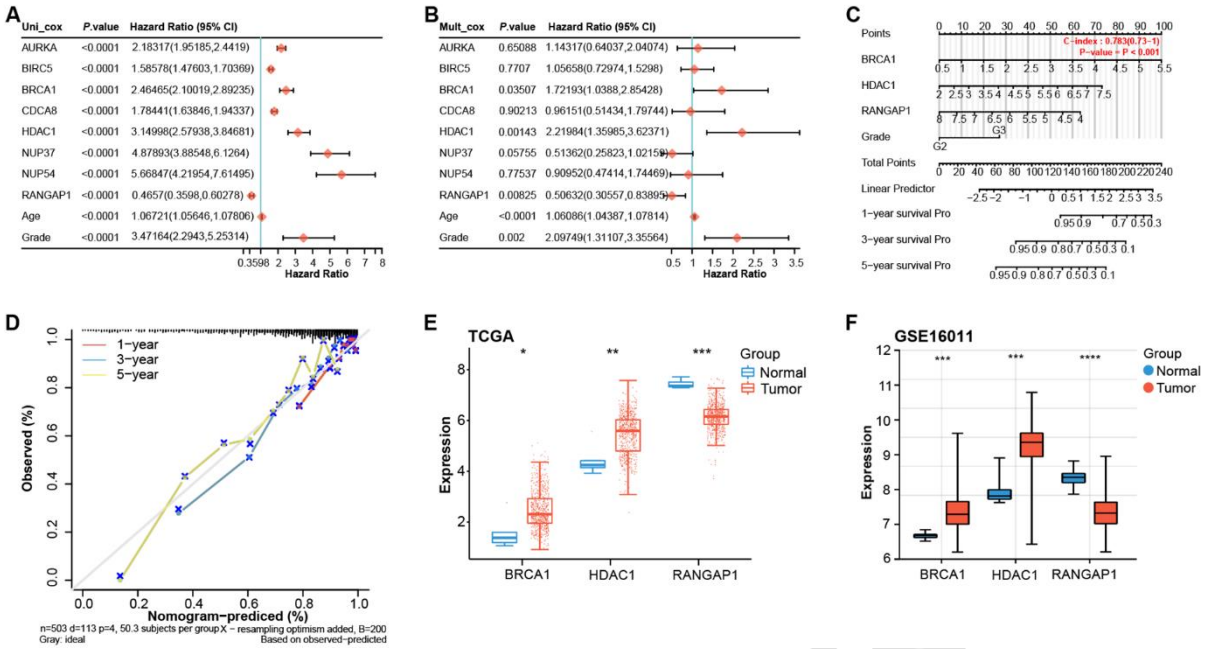

Figure 3. **Prognostic analysis of gene expression and clinical factors in glioma.** (A and B) Univariate/multifactorial Cox regression analysis on signature genes and clinical prognostic variables. The significance of each factor in relation to overall survival is indicated by the p value. (C) Nomogram of key prognostic variables and C-index used to evaluate the predictive ability of the model at 1, 3, and 5-years survival. (D) The dashed line indicates the ideal calibration curve of the nomogram with the red dash, blue dash, and yellow dash for the 1-year, 3-year, and 5-year predictions, respectively. (E and F) Box plot of expression analysis of three key genes in TCGA-glioma and GSE16011 dataset. Among them, blue represents normal samples and red represents tumor samples. *p<0.05, **p<0.01, ***p<0.001, ****p<0.0001.

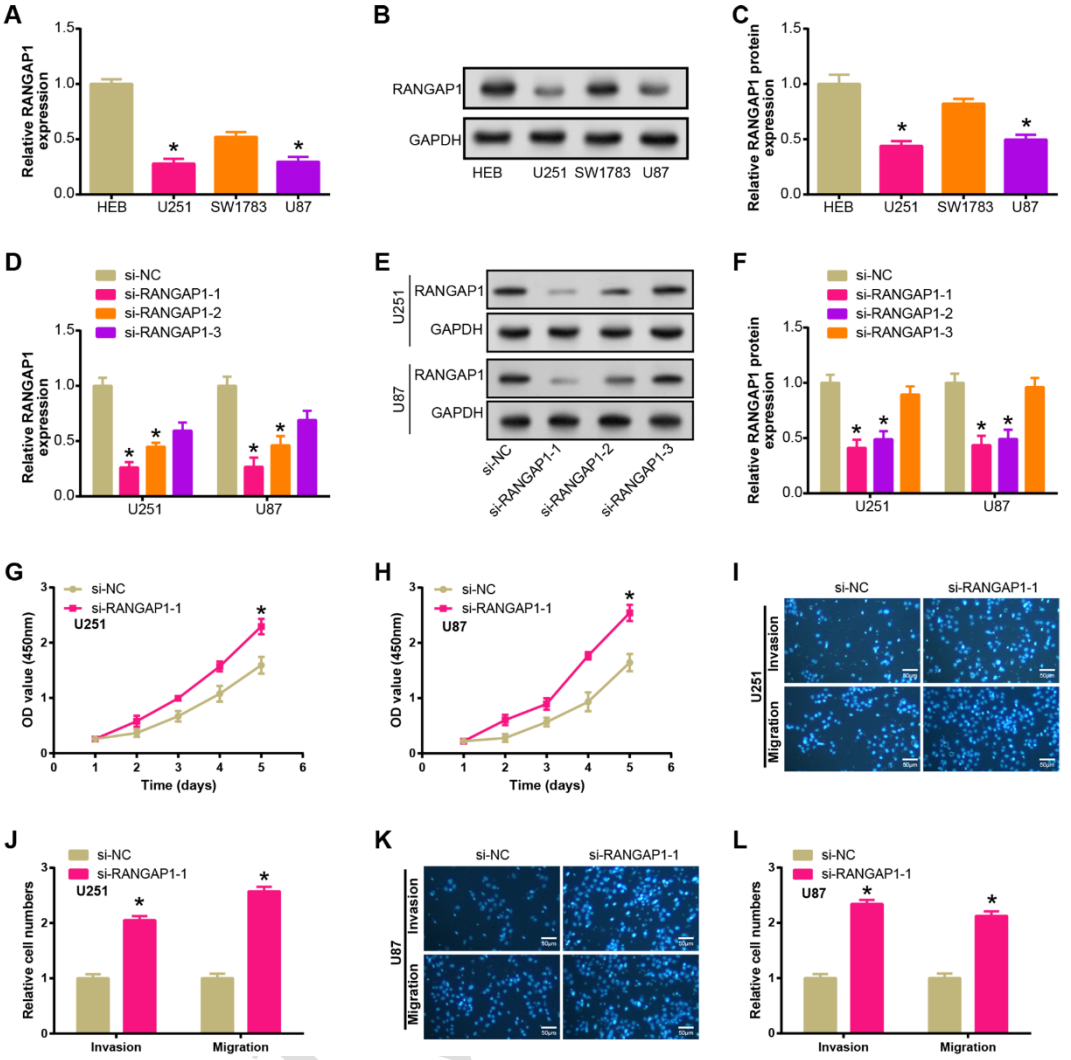

Figure 4. Downregulation of RANGAP1 promotes proliferation, migration, and invasion of glioma cells. (A-C) qRT-PCR and WB detected the expression of RANGAP1 in normal brain glial cells (HEB) and glioma cells (U251, SW1783, and U87). (D-F) qRT-PCR and WB detected the knockdown efficiency of RANGAP1(si-RANGAP1-1, si-RANGAP1-2, si-RANGAP1-3) in glioma cells (U251 and U87). (G and H) CCK8 detects the effect of si-RANGAP1-1 on U251 and U87 cell proliferation. Green represents si-NC group, and red represents si-RANGAP-1 group. (I-L) Transwell detects the effect of si-RANGAP1-1 on the invasion and migration numbers of U251 and U87 cells. Scale bar is 50 μm. *p<0.05. Each experiment was replicated three times.

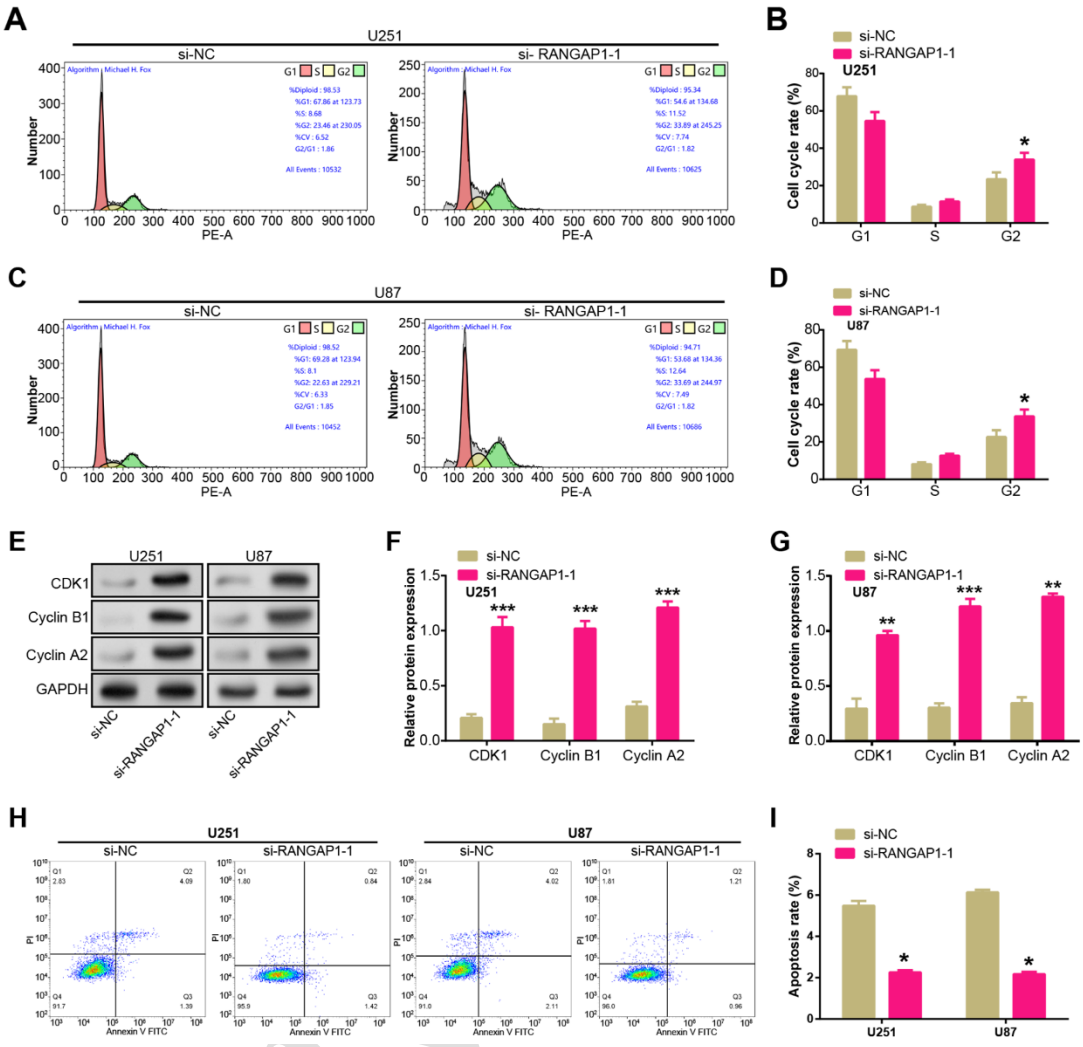

Figure 5. RANGAP1 knockdown disrupts cell cycle distribution and inhibits apoptosis in U251 and U87 cells. (A-D) Flow cytometry to detect the effect of si-RANGAP1-1 on the cell cycle of U251 and U87 cells. (E-G) WB detection of the effect of si-RANGAP1-1 on cell cycle proteins (CDK1, Cyclin B1, Cyclin A2) in U251 and U87 cells. (H and I) Flow cytometry to detect the effect of si-RANGAP1-1 on apoptosis of U251 and U87 cells. *p<0.05. Each experiment was replicated three times.

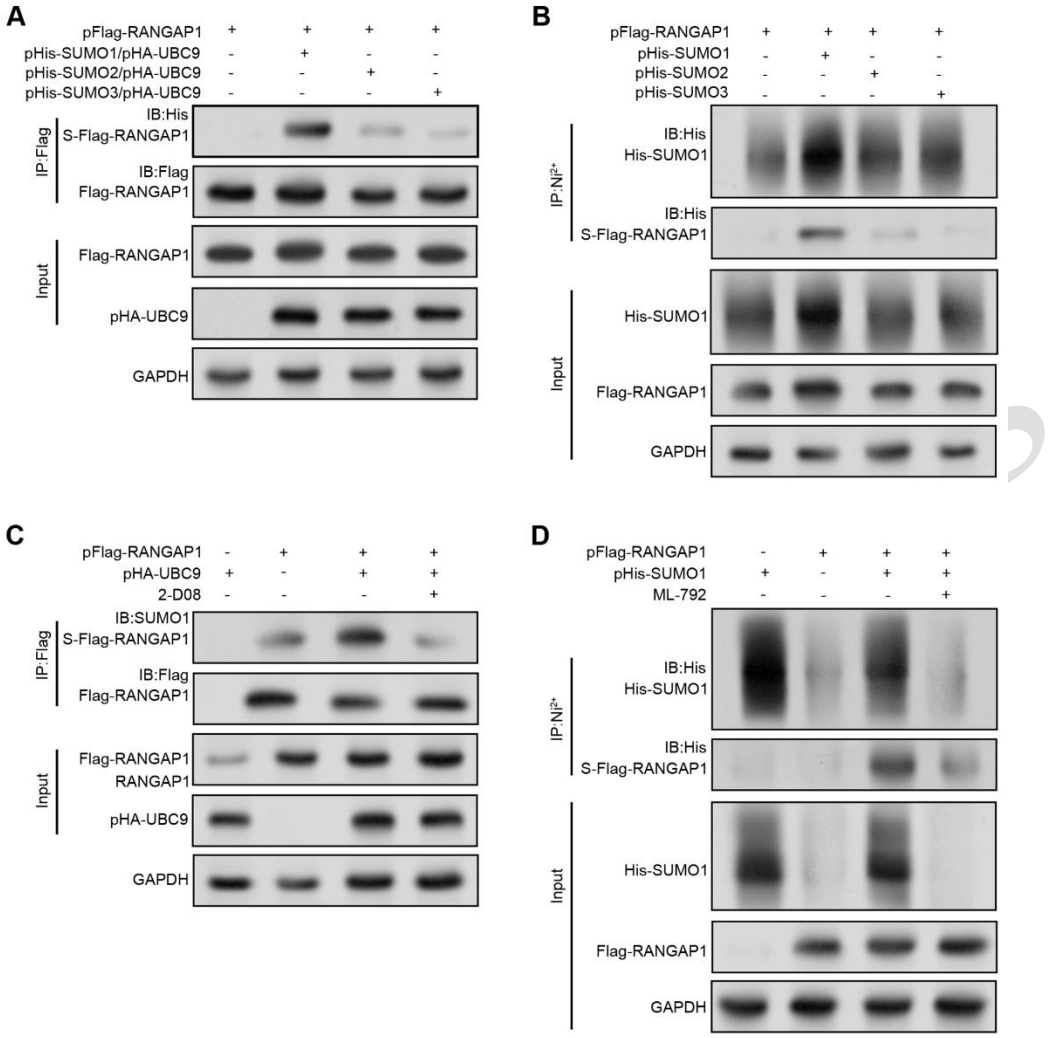

Figure 6. SUMO1 conjugation modifies RANGAP1. (A) WB analysis of RANGAP1 SUMOylation following co-immunoprecipitation with HA-tagged UBC9 and His-tagged SUMO proteins in HEK293T cells. Anti-His antibody detects SUMOylated RANGAP1 after Flag immunoprecipitation. The lower panels show total RANGAP1 and HA-UBC9 levels in the initial lysates with GAPDH serving as a loading control. (B) His-tag affinity purification of SUMOylated proteins demonstrates the specific SUMOylation of Flag-RANGAP1 in the presence of His-SUMO1, His-SUMO2, and His-SUMO3. (C and D) The SUMOylation of RANGAP1 was examined in response to UBC9/SUMO1 enhancement or inhibitor treatment (2-D08 or ML-792). HEK293T cells were co-transfected with pFlag-RANGAP1 and pHA-

UBC9 or pHis-SUMO1 plasmids, followed by treatment with 150 μM 2-D08 (C) or 10 μM ML-792 (D) for an additional 24 hours. Immunoprecipitation using anti-Flag antibody-coupled agarose beads (C) or Ni2+-NTA agarose beads (D) enriched the Flag-tagged RANGAP1 protein, allowing analysis of SUMOylated RANGAP1 levels by WB assay using Flag or SUMO1 antibodies. S-Flag-RANGAP1 denotes SUMOylated Flag-tagged RANGAP1, and Input refers to an equivalent amount of cell lysate loaded. 2-D08 or ML-792 serves as a SUMOylation inhibitor. Each experiment was replicated three times.

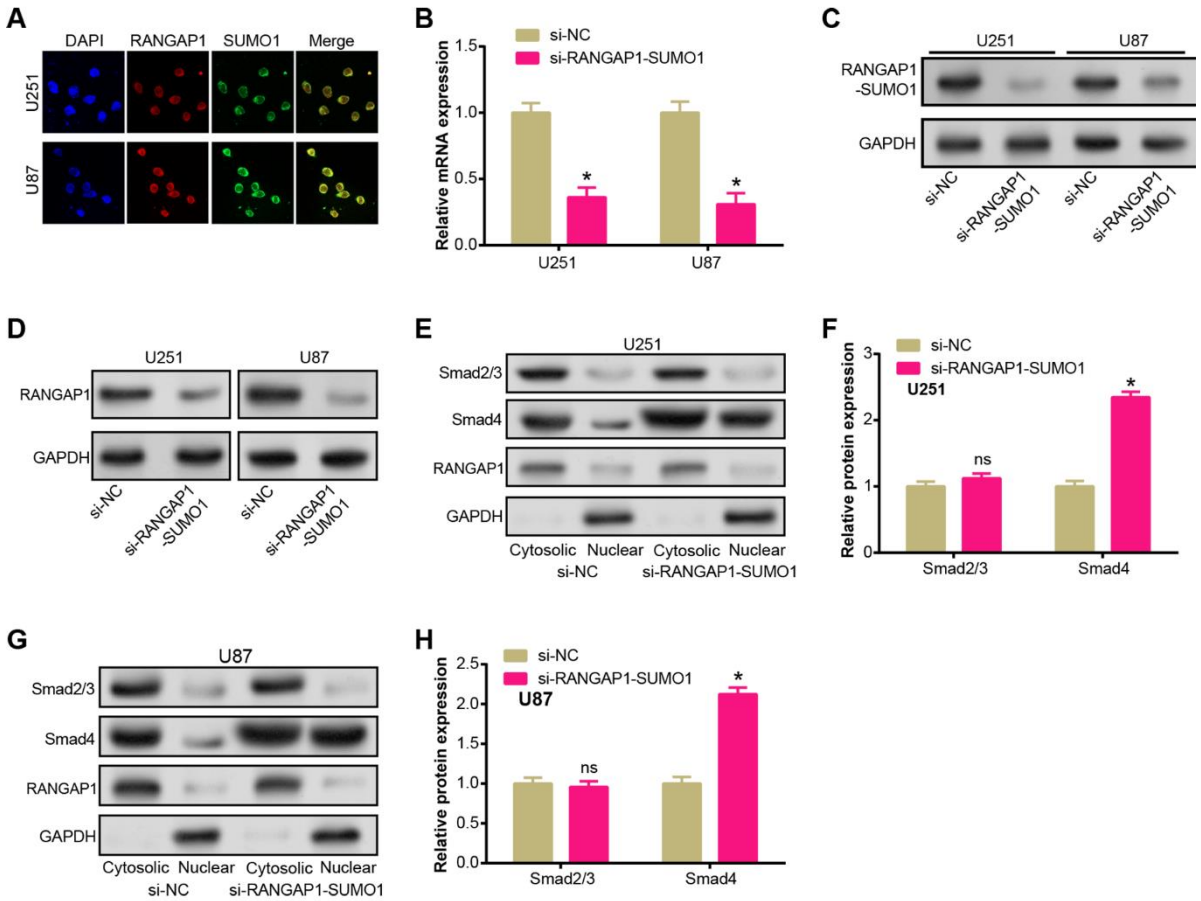

Figure 7. Knockdown of SUMO1 affects the nucleocytoplasmic distribution of Smad4 in the TGF-β/Smad signaling pathway. (A) Immunofluorescence staining of U251 and U87 cells displaying the localization of RANGAP1 (red), SUMO1 (green), and the nucleus (DAPI,

blue). The merged images show the colocalization of RANGAP1 and SUMO1 within the cells. (B and C) qRT-PCR and WB detected the transfection efficiency of siRNA targeting RANGAP1-SUMO1 complex (si-RANGAP1-SUMO1) in glioma cells. (D) WB detection of RANGAP1 expression changes after RANGAP1-SUMO1 complex knockdown in glioma cells (U251 and U87). (E-H) WB detects the expression changes of Smad2/3 and Smad4 in the nucleoplasm of U251 and U87 cells after RANGAP1-SUMO1 complex knockdown. ns: not significant, *p<0.05. Each experiment was replicated three times.

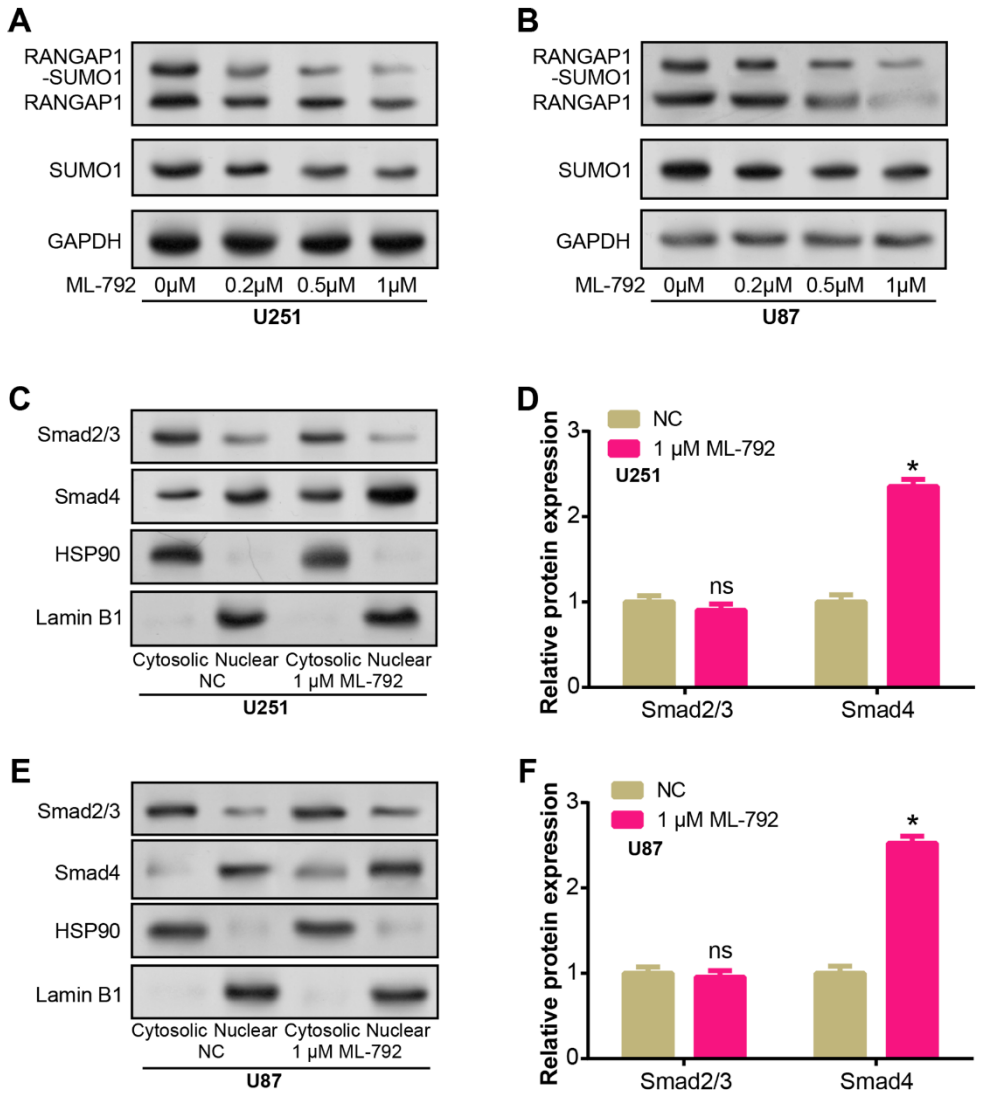

Figure 8. RANGAP1-SUMO1 affects the nuclear export of Smad4. (A and B) U87 and U251 cells were treated with a certain concentration gradient of ML-792 (inhibitor) for 2 h, and the inhibitory effect of ML-792 on RANGAP1-SUMO1 complex, RANGAP1 and free SUMO1 was evaluated by WB. (C-F) WB detection of nucleoplasmic expression levels of Smad2/3 and Smad4 after U87 and U251 cells were treated with 1 μM ML-792 for 2 hours. HSP90 and Lamin B1 are reference proteins in the cytosol and nucleus, respectively. ns: not significant, *p<0.05. Each experiment was replicated three times.

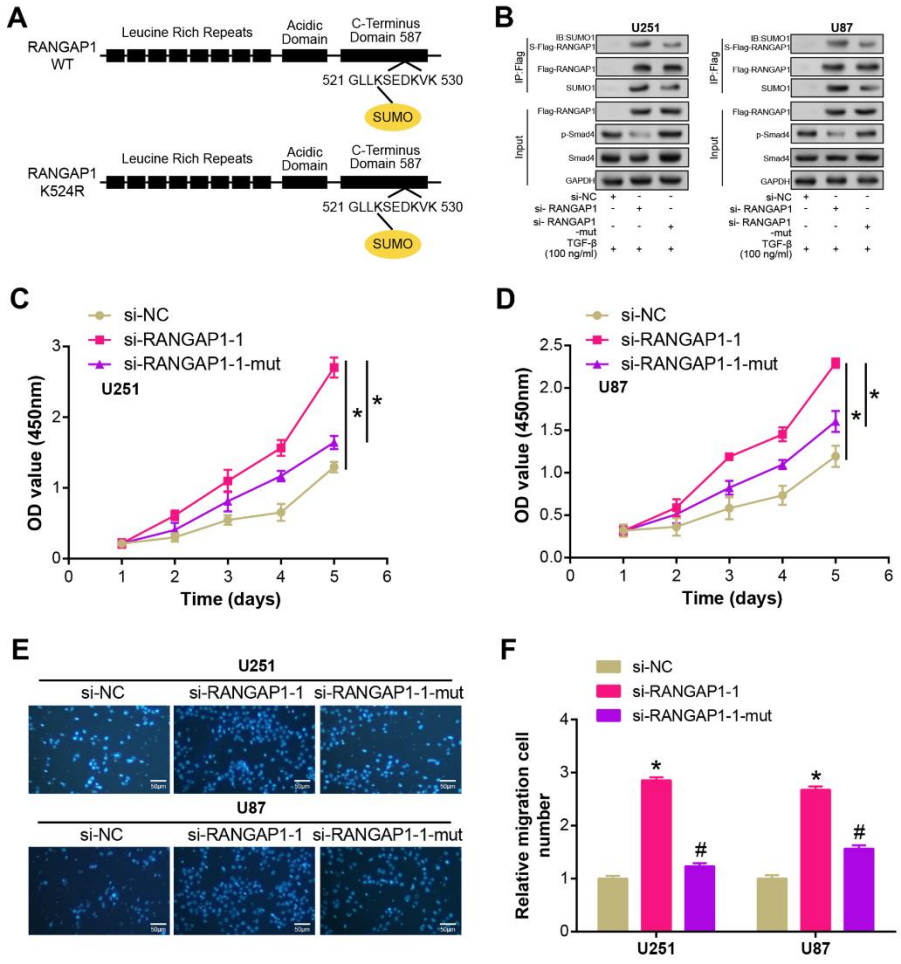

Figure 9. RANGAP1 SUMOylation affects Smad4 to hinder cell proliferation and migration. (A) Schematic representation of wild-type RANGAP1 (WT) and the RANGAP1

K524R mutant depicting the leucine-rich repeats, acidic domain, C-terminus, and SUMO modification site. (B) WB analysis after immunoprecipitation showing SUMO1 conjugation to RANGAP1 in U251 and U87 cells. Cells were transfected with si-NC, si-RANGAP1, or si-RANGAP1 in combination with SUMO1 under TGF-β stimulation. The phosphorylation status of Smad4 and total Smad4 levels were assessed. (C and D) Cell proliferation assays measuring the optical density (OD) at 450 nm of U251 (C) and U87 (D) cells transfected with si-NC, si-RANGAP1-1, or si-RANGAP1-1-mut over 5 days. (E and F) Transwell migration assays of U251 and U87 cells transfected with si-NC, si-RANGAP1-1, or si-RANGAP1-1-mut. *$p<0.05$, #$p<0.05$. Each experiment was replicated three times.

SUPPLEMENTAL DATA

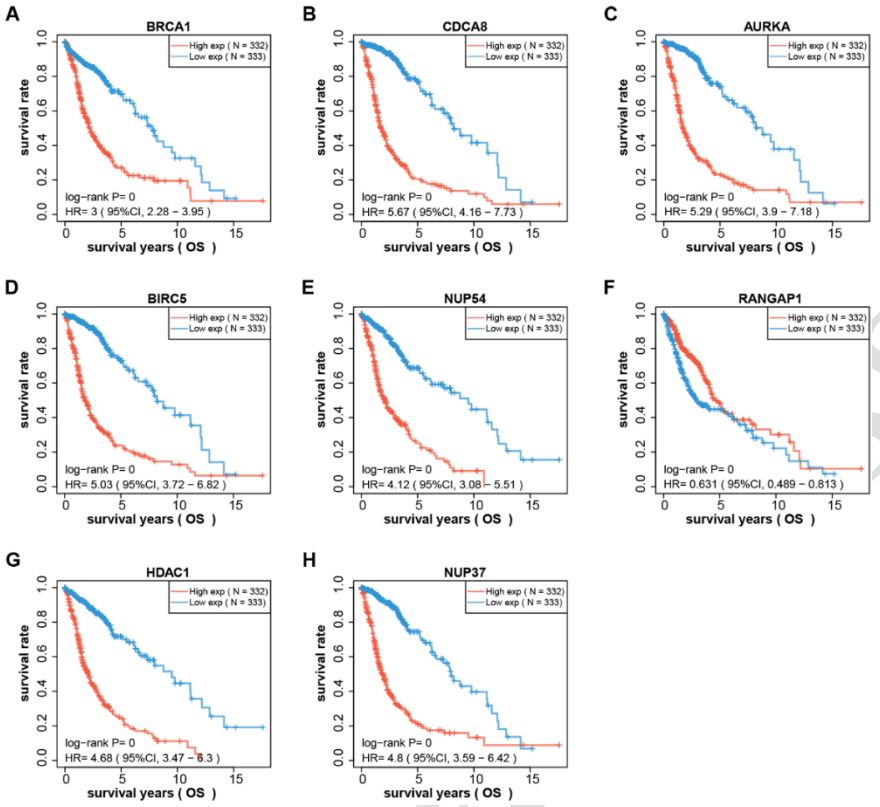

Figure S1. OS prognosis of 8 prognostically significant genes in glioma. (A-H) KM survival curve chart, overall survival (OS) probability of patients with high and low gene expression during 15 years. Red represents high expression and blue represents low expression. Genes analyzed were as follows: BRCA1 (A), CDCAB8 (B), AURKA (C), BIRC5 (D), NUP54 (E), RANGAP1 (F), HDAC1 (G), and NUP37 (H).

Supplementary table is available at the following link:

https://www.bjbms.org/ojs/index.php/bjbms/article/view/10443/3289